Journal of Alloys and Compounds 509 (2011) 6864–6870

Contents lists available at ScienceDirect

Journal of Alloys and Compounds

journal homepage: www.elsevier.com/locate/jallcom

Synthesis and crystallization behavior of 3 mol% yttria stabilized tetragonal zirconia polycrystals (3Y-TZP) nanosized powders prepared using a simple co-precipitation process

Yu-Wei Hsu[a], Ko-Ho Yang[a,b,**], Kuo-Ming Chang[c,d], Sung-Wei Yeh[e], Moo-Chin Wang[f,*]

[a] Graduate Institute of Applied Science, National Kaohsiung University of Applied Sciences, 415 Chien-Kung Road, Kaohsiung 80782, Taiwan
[b] Department of Mold and Die Engineering, National Kaohsiung University of Applied Sciences, 415 Chien-Kung Road, Kaohsiung 80782, Taiwan
[c] Department of Mechanical Engineering, National Kaohsiung University of Applied Sciences, 415 Chien-Kung Road, Kaohsiung 80782, Taiwan
[d] Dental Materials Research Center, National Kaohsiung University of Applied Sciences, 415 Chien-Kung Road, Kaohsiung 80782, Taiwan
[e] Metal Industries Research and Development Centre, 1001 Kaohsiung Highway, Kaohsiung 811, Taiwan
[f] Department of Fragrance and Cosmetics Science, Kaohsiung Medical University, 100, Shihchuan 1st Road, Kaohsiung 80728, Taiwan

ARTICLE INFO

Article history:
Received 20 February 2011
Accepted 26 March 2011
Available online 5 April 2011

Keywords:
Co-precipitation process
Crystallization behavior
Non-isothermal method
Plate-like morphology

ABSTRACT

The synthesis and crystallization behavior of 3 mol% yttria stabilized tetragonal zirconia polycrystals (3Y-TZP) nanopowders prepared using a simple co-precipitation process at 348 K and pH = 7 were investigated using differential scanning calorimetry/thermogravimetry (DSC/TG), an X-ray diffractometer (XRD), the Raman spectra, transmission electron microscopy (TEM), selected area electron diffraction (SAED), and an energy dispersive spectrometer (EDS). The activation energy of tetragonal ZrO_2 crystallization from 3Y-TZP freeze-dried precursor powders using a non-isothermal method, namely, $169.2 \pm 21.9\ kJ\ mol^{-1}$, was obtained. The growth morphology parameter n was approximated as 2.0, which indicated that it had a plate-like morphology. The XRD, Raman spectra, and SAED patterns showed that the phase of the tetragonal ZrO_2 was maintained at 1273 K. The crystallite size of 3Y-TZP freeze-dried precursor powders calcined at 1273 K for 5 min was 21.3 nm.

1. Introduction

Zirconia is generally found in zircon ($ZrSiO_4$) and baddeleyite in the nature and is a common ceramic material. Zirconia has three polymorph forms: monoclinic (M), tetragonal (T) and cubic (C) [1]. At temperatures lower than 1443 K pure zirconia is in the monoclinic phase. At temperatures from 1443 to 2643 K zirconia is in the tetragonal phase. And at temperatures above 2643 K zirconia is in the cubic phase [2]. Moreover, pure zirconia ceramics can move from the tetragonal phase to the monoclinic phase, which is accompanied by variation in volume, through a spontaneous stress-induced martensitic transformation when cooling from a high temperature to room temperature. To avoid phase transformation, Pascual and Duran [3] proposed that 8 mol% yttria stabilized zirconia (8YSZ) ceramics with a single cubic phase (fully stabilized zirconia, FSZ) is desirable for high temperature applications. The addition of 3–6 mol% yttria to zirconia can make the tetragonal phase the primary phase.

When the component phases of zirconia are multi-phase (i.e. both the tetragonal and monoclinic phases exist in matrix) this is called partially stabilized zirconia (PSZ). Tetragonal zirconia polycrystals (TZP) is zirconia in which the component phase is almost tetragonal. Both PSZ and TZP possess excellent mechanical properties, especially fracture toughness. Toughness differs from brittleness of in common ceramics [4] and is the result of three types of toughening mechanisms in tetragonal zirconia. The first type is the transformation toughening mechanism, which was proposed by Green et al. [5] and Hannink et al. [6]. The microcracking toughening mechanism is the second type toughening mechanism, which was proposed by Claussen et al. [7] and Evans and Cannon [8]. The third toughening mechanism was proposed by Virkar et al. [8–11]. He proposed that tetragonal ZrO_2 become tougher after stress-induced domain switching.

Recently, various processes have been widely used for synthesizing YSZ nano-particles which have been reported, such as the co-precipitation [12], hydrothermal [13], and sol–gel processes [14]. The co-precipitation process has the advantages of low cost, easy-to-acquire equipments, a well-mixed solution, and nanometric precursor particles. Through frozen and dried processes the YSZ amorphous precursor powders become crystalline YSZ powders after calcinaiton. The activation energies of the crystallization of Y-TZP prepared using with and without seeding-assisted

* Corresponding author. Tel.: +886 7 3121101x2366; fax: +886 7 3210683.
** Corresponding author. Tel.: +886 7 3814526x5403.
E-mail addresses: yangkoho@cc.kuas.edu.tw (K.H. Yang), mcwang@kmu.edu.tw (M.C. Wang).

0925-8388/$ – see front matter © 2011 Elsevier B.V. All rights reserved.
doi:10.1016/j.jallcom.2011.03.162

chemical co-precipitation were reported by Durán et al. [15]. They proposed that the addition of nanosized Y-TZP amorphous precursors created the apparent activation energy decreased from 184 to 119 kJ mol^{-1} for the Y-TZP crystallization. However, the crystallization behavior and crystallite growth mechanism have not been discussed in detail. In addition, Kuo et al. [16] also reported that the activation energy of cubic ZrO_2 formation in 8YSZ using the non-isothermal method is 231.76 kJ mol^{-1}, and that the crystallite growth mechanism belongs to 3-dimensional growth. However, although 3Y-TZP has important applications in many fields, including the manufacture of biomaterials and dental materials [17], its crystallization behavior has not been elaborated on.

In the present study, the synthesis and crystallization behavior of 3 mol% yttria stabilized tetragonal zirconia (3Y-TZP) precursor powders prepared from zirconium nitrate and yttrium nitrate hexahydrate using a simple co-precipitation process were investigated using differential scanning calorimetry/thermogravimetry (DSC/TG), an X-ray diffractometer (XRD), the Raman spectra, transmission electron microscopy (TEM), selected area electron diffraction (SAED), and an energy dispersive spectrometer (EDS).

The purpose of the present study was: (i) to study the thermal behavior of 3Y-TZP freeze-dried precursor powders, (ii) to study the crystallization behavior of 3Y-TZP freeze-dried precursor powders after they have been calcined, and (iii) to observe the microstructure of calcined 3Y-TZP powders.

2. Experimental procedures

2.1. Sample preparation

Zirconium (IV) nitrate ($Zr(NO_3)_4{\cdot}xH_2O$ purity ~ 99.5%, supplied by Acros Organics, Belgium) and yttrium nitrate hexahydrate ($Y(NO_3)_3{\cdot}6H_2O$, purity ~ 99.9%, supplied by Acros Organics, Belgium) were used in this study. The polyethylene glycol (PEG, MW 6000, supplied by Nippon Shiyaku Kogyo K.K, Japan) was used as a dispersant. Zirconium nitrate and yttrium nitrate were dissolved in a solution of deionized water and ethanol at a volume ratio of 1:5. The ratio of Y_2O_3 to ($Y_2O_3 + ZrO_2$) equal to 3 mol% in solution was prepared, and 1 wt% PEG was added to reduce agglomeration. The mixed solution was stirred using a magnetic stirrer and heated to 348 K. NH_4OH (Nihon Shiyaku Reagent, Japan) and was then slowly added to the solution until it reached a pH of 7. After precipitation, the precipitates were repeatedly rinsed with a large amount of deionized water through ultrasonic sieving, and then the precursor powders were freeze-dried at 223 K in a vacuum.

2.2. Sample characterization

A DSC/TG (SDT Q600, TA, USA) was conducted in the temperature range 323–1273 K in static air. Approximately 8 mg of freeze-dried precursor powders were heated at various rates. Al_2O_3 powders were used as a reference material. The calcination temperature was determined from the DSC results.

The crystalline phase was identified by XRD (D8 Advance, Bruker, Germany) with Cu Kα radiation and a Ni filter operating at 40 kV, 40 mA, and scanning at a rate of 1° min^{-1}. The Raman spectroscopy (HR800, HORIBA, Japan) was identified at room temperature with a 633 nm excitation line of a diode-pumped solid state laser.

The morphology of the 3Y-PSZ precursor powders was examined by TEM (JEM 2100F, JEOL, Japan) operating at 200 kV. SAED and EDS (INCA TEM250, Oxford, UK) examinations were also done on the powders.

3. Results and discussion

3.1. Thermal behavior of freeze-dried precursor powders

The DSC/TG curve of the 3Y-PSZ precursor powders heated at a rate of 5 K min^{-1} are shown in Fig. 1. The TG curve can be divided to four major weight loss stages: (i) 298–357 K (ii) 357–453 K (iii) 453–613 K and (iv) 613–1020 K. In the first stage, about 6.5% of the weight loss was attributed to the evaporation of water on the surfaces of the precursor powders. In the second stage, 357–453 K, about 10.6% weight loss was caused by the follow reaction:

$$\underset{(ZrO_2 \cdot H_2O)}{[Zr_4(OH)_8][OH]_8} \rightarrow \underset{(ZrO_2 \cdot 2H_2O)}{[Zr_4(OH)_4O_4][OH]_4} + 4H_2O \quad (1)$$

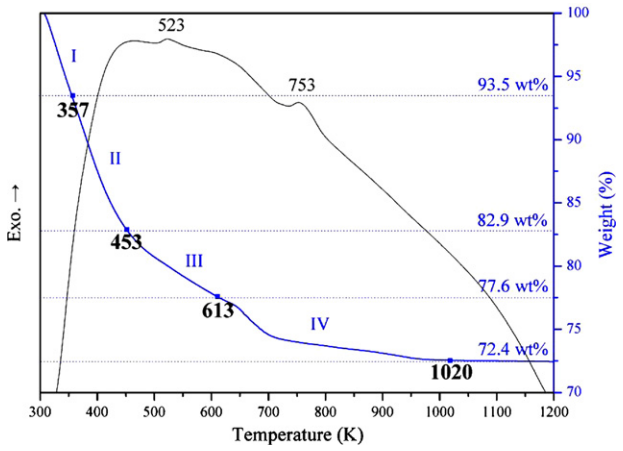

Fig. 1. The DSC/TG curves for 3Y-TZP freeze-dried precursor powders heated at a rate of 5 K min^{-1} from 300 to 1200 K.

This is because the square-arranged Zr atoms were linked by four OH groups and four O atoms in the $[Zr_4(OH)_4O_4]^{4+}$ cation. In the third stage, 453–613 K, a weight loss of about 5.3% was caused by the reaction from $ZrO_2{\cdot}H_2O$ lost $1/2H_2O$. The reaction is as follows:

$$\underset{\left(ZrO_2 \cdot \frac{1}{2}H_2O\right)}{[Zr_4(OH)_4O_4][OH]_4} \rightarrow [Zr_4(OH)_2O_6][OH]_2 + 2H_2O \quad (2)$$

In the fourth stage, 613–1020 K, the transformation of $ZrO_2{\cdot}1/2H_2O$ to ZrO_2 crystallites occurred, resulting in about 5.2% weight loss. This was the final dehydration reaction:

$$[Zr_4(OH)_2O_6][OH]_2 \rightarrow 4ZrO_2 + 2H_2O \quad (3)$$

Whitney [18] pointed out that the $ZrO_2{\cdot}6H_2O$, which corresponds to residual 53 wt% ZrO_2, is the product of a metathetical reaction between the base and zirconyl ions. In the present study, the freeze-dried precursor powders contained about 72.4 wt% ZrO_2, which corresponds to $ZrO_2{\cdot}2H_2O$.

In addition, the DSC curve of the 3Y-TZP freeze-dried precursor powders at a heating rate of 5 K min^{-1} in static air also shows two exothermic peaks, one at 523 K and the other one at 753 K. The first exothermic peak at 523 K was caused by the dehydration reaction leading to the atomic prearrangement of the tetragonal structure which caused the 3Y-TZP freeze-dried precursor powders to approach a more stable state [19]. Furthermore, the second exothermic peak, which appeared at 753 K, was caused by the crystalline ZrO_2 formation of the amorphous 3Y-TZP freeze-dried precursor powders.

3.2. The crystal structure of 3Y-TZP freeze-dried precursor powders after calcination

The typical XRD patterns of 3Y-TZP freeze-dried precursor powders calcined at various temperatures for 5 min are shown in Fig. 2. The XRD pattern of uncalcined freeze-dried precursor powders shows that no reflection peak can be found. This result shows that the freeze-dried precursor powders maintained their amorphous states. No reflection peak was found in the XRD patterns of the 3Y-TZP freeze-dried powders calcined at 573 and 673 K for 5 min. This result can be attributed to the freeze-dried precursor powders calcined 573 and 673 K for 5 min also maintaining their amorphous states. When calcined at 773 K for 5 min, the reflection peaks of the XRD pattern first displayed the tetragonal ZrO_2 phase. When the 3Y-TZP freeze-dried precursor powders calcined at 1073

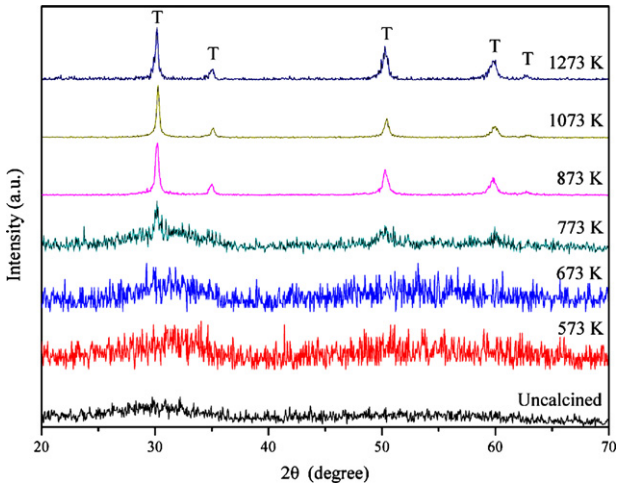

Fig. 2. Typical broad-scan XRD patterns of 3Y-TZP uncalcined freeze-dried precursor powders and freeze-dried precursor powders calcined at various temperatures for 5 min. "T" denotes the tetragonal ZrO_2 phase.

and 1273 K, respectively, for 5 min, the XRD patterns still revealed tetragonal ZrO_2.

According to the results of Fig. 1, the second exothermic peak temperature of the 3Y-TZP precursor freeze-dried powders appeared at 753 K. This result shows that the second exothermic peak temperature corresponded to the tetragonal ZrO_2 formation of the 3Y-TZP freeze-dried precursor powders. In addition, the XRD patterns showed that all the reflection peaks maintained the tetragonal ZrO_2 phase and that the intensity of the reflection peaks increased with the temperature when the freeze-dried precursor powders calcined between 873 and 1273 K for 5 min, i.e. the crystallity of the 3Y-TZP powders improved as the calcined temperature increased.

Fig. 3 shows the Raman spectra of uncalcined 3Y-TZP freeze-dried precursor powders calcined at various temperatures for 5 min. Two broad peaks appeared at about 265 and 290 cm^{-1}, respectively. The results of Fig. 3 show that all the peaks belonged to the tetragonal phase [20]. Furthermore, the peak-broadening phenomenon in Fig. 3 was probably caused by disordered lattice defects [21].

A comparison of the results of Figs. 2 and 3 shows that, although the XRD results for the uncalcined 3Y-TZP freeze-dried precursor powders calcined at 573 and 673 K for 5 min indicate that they maintained an amorphous state, the Raman spectra of the uncalcined 3Y-TZP freeze-dried precursor powders shows that the tetragonal ZrO_2 phase could be attributed to the tetragonal phase already having been formed. The metastable tetragonal phase could be stabilized at room temperature by doping yttrium cations into the ZrO_2 lattice [22]. Monoclinic is the most stable crystal structure at room temperature for pure ZrO_2 because it favors 7-fold Zr–O coordination. When less than four valences cations, such as Y^{3+}, are doped into the ZrO_2 lattice, oxygen vacancies are generated for the charge balance of the structure. Because the radius of Y^{3+} (1.02 Å) is larger than that of Zr^{4+} (0.84 Å), the oxygen vacancies tend to be associated with Zr^{4+}. This makes the effective coordination number less than 7. For maintaining the coordination number to approach to 7, the ZrO_2 changes the lattice structure to an 8-fold coordination, which leads to the formation of tetragonal or cubic structures [23].

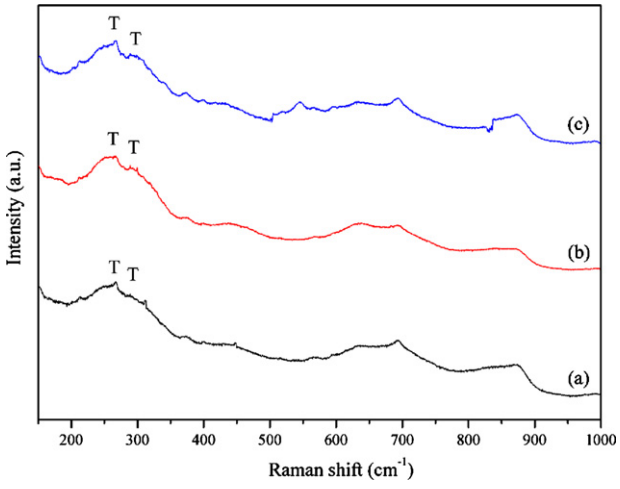

Fig. 3. The Raman spectra of 3Y-TZP freeze-dried precursor powders: (a) uncalcined (b) calcined at 773 K, and (c) calcined at 1273 K for 5 min. "T" denotes the tetragonal ZrO_2 phase.

On the other hand, Clearfield [24] points out that, since the dissolution/precipitation the hydrous zirconia is a slow process resulting in the formation of ordered sheets and leading to the tetragonal phase through self-assembly, even XRD patterns show the amorphous state. Denkewicz et al. [25] also presented a similar point of view regarding amorphous precursor ($Zr(OH)_xO_y$) losing structural water during calcination, and then transforming into polycrystalline aggregated tetragonal zirconia. In addition, Chuah [26] also proposed that hydrous zirconia digested by reflux undergoes a dehydration process and generally forms a more stable framework structure than amorphous hydrous zirconia, and then transitions into the tetragonal phase through topotactic rearrangement after calcination. The existence of a more stable framework structure can be confirmed by decreasing the enthalpy and the increasing activation energy of the crystallization process. The results of the present study correspond with the results of Clearfield [24] and Denkewicz et al. [25].

In addition, Sato et al. [21] dissolved $ZrOCl_2{\cdot}8H_2O$ in a $KHCO_3$/KOH solution, and obtained full tetragonal zirconia after a hydrothermal process. In the present study, full tetragonal zirconia was also obtained using a simple co-precipitation process at normal atmospheric pressure.

3.3. The crystallization behavior of 3Y-TZP freeze-dried precursor powders

The DSC curves of the 3Y-TZP freeze-dried precursor powders at various heating rate in static air are shown in Fig. 4. Each curve has two exothermic peaks. The first exothermic peak temperatures are between 523 and 561 K, and the second exothermic peak temperatures are between 753 and 793 K. In addition, Fig. 4 also shows that the exothermic peaks shift to higher temperatures when the heating rate is increased. This phenomenon can be attributed to the high heating rates resulting in the transition temperature leaving the equilibrium transition point leading it to shift to a higher temperature.

The exothermic peak temperatures of the DSC curves can be used to research crystallization kinetics using a non-isothermal method. In the present study, the Johnson–Mehl–Avrami (JMA) equation was applied to derive the non-isothermal activation energy of the phase crystallization from the 3Y-PSZ freeze-dried precursor powders [27];

$$\ln \beta = -\frac{E_c}{RT_c} + \ln CM \tag{4}$$

where β means the heating rate, E_c denotes the crystallization activation energy, R is the gas constant, T_c is the temperature that corresponds to the exothermic peak of crystallization, and In CM is a constant.

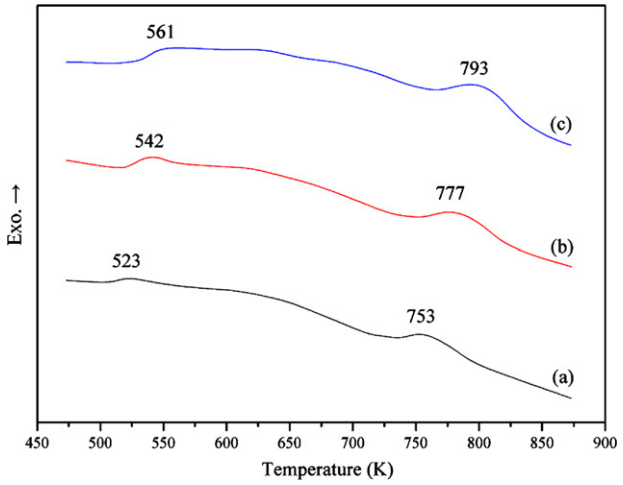

Fig. 4. DSC curves of the 3Y-TZP freeze-dried precursor powders at various heating rates: (a) 5, (b) 10 and (c) 20 K min^{-1}.

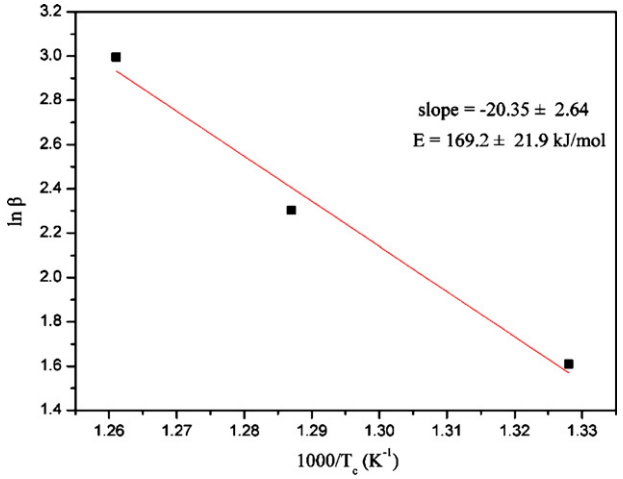

Fig. 5. Plots of lnβ versus $1/T_c$ for 3Y-TZP nano-powders.

Fig. 5 shows the result of lnβ versus $(1/T_c)$ for 3Y-TZP freeze-dried precursor powders. The slope of the fitting line of the plots was -20.35 ± 2.64. After calculations, the activation energy, 169.2 ± 21.9 kJ mol^{-1} for tetragonal ZrO_2 crystallization from 3Y-TZP freeze-dried precursor powders was obtained. This value approached to the crystallization activation energy of 3Y-TZP, 184 kJ mol^{-1}, prepared using a co-precipitation process that used $(Zr(C_4H_9O)_4{\cdot}C_4H_9OH)$ and solvent (2-propanol) as the start materials [15].

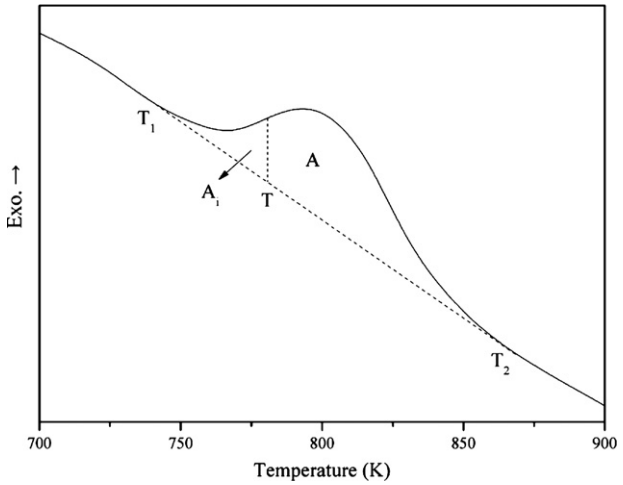

Fig. 6. An enlarged view of the exothermic peak of the DSC curves for 3Y-TZP freeze-dried precursor powders heated at a rate of 20 K min^{-1}.

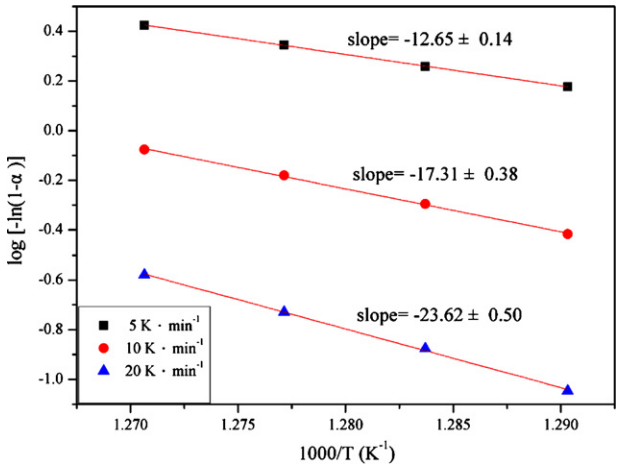

Fig. 7. Plots for log[$-\ln(1-\alpha)$] versus $1/T$ at various heating rates for 3Y-TZP nano-powders.

In addition, Durán et al. [15] also pointed out that the crystallization activation energy of 3Y-TZP amorphous powders prepared by seeding-assisted chemical co-precipitation was 119 kJ mol^{-1}. The difference between the results obtained by Durán et al. [15] and those in the present study could have been caused by the using seeding-assisted chemical co-precipitation providing the heterogeneous nucleation sites and leading to the a decrease in crystallization activation energy. On the other hand, the crystallization activation energy of the transformation from the amorphous phase to the tetragonal (169.2 kJ mol^{-1}) was smaller than that of the transformation to the cubic (231.76 kJ mol^{-1}) [16]. This result shows that yttria stabilized zirconia materials require less energy to transform to the tetragonal phase than to the cubic.

When the 3Y-TZP freeze-dried precursor powders were heated at a constant rate, β, over a period of time from room temperature (T_r) to a certain temperature (T), the total number of nuclei, N, took shape per volume and the radius of crystallites, r, were presented

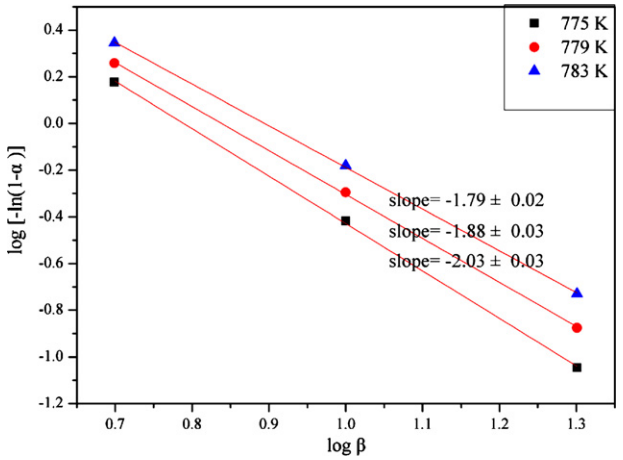

Fig. 8. Plots for log[$-\ln(1-\alpha)$] versus logβ at different temperatures for 3Y-TZP nano-powders.

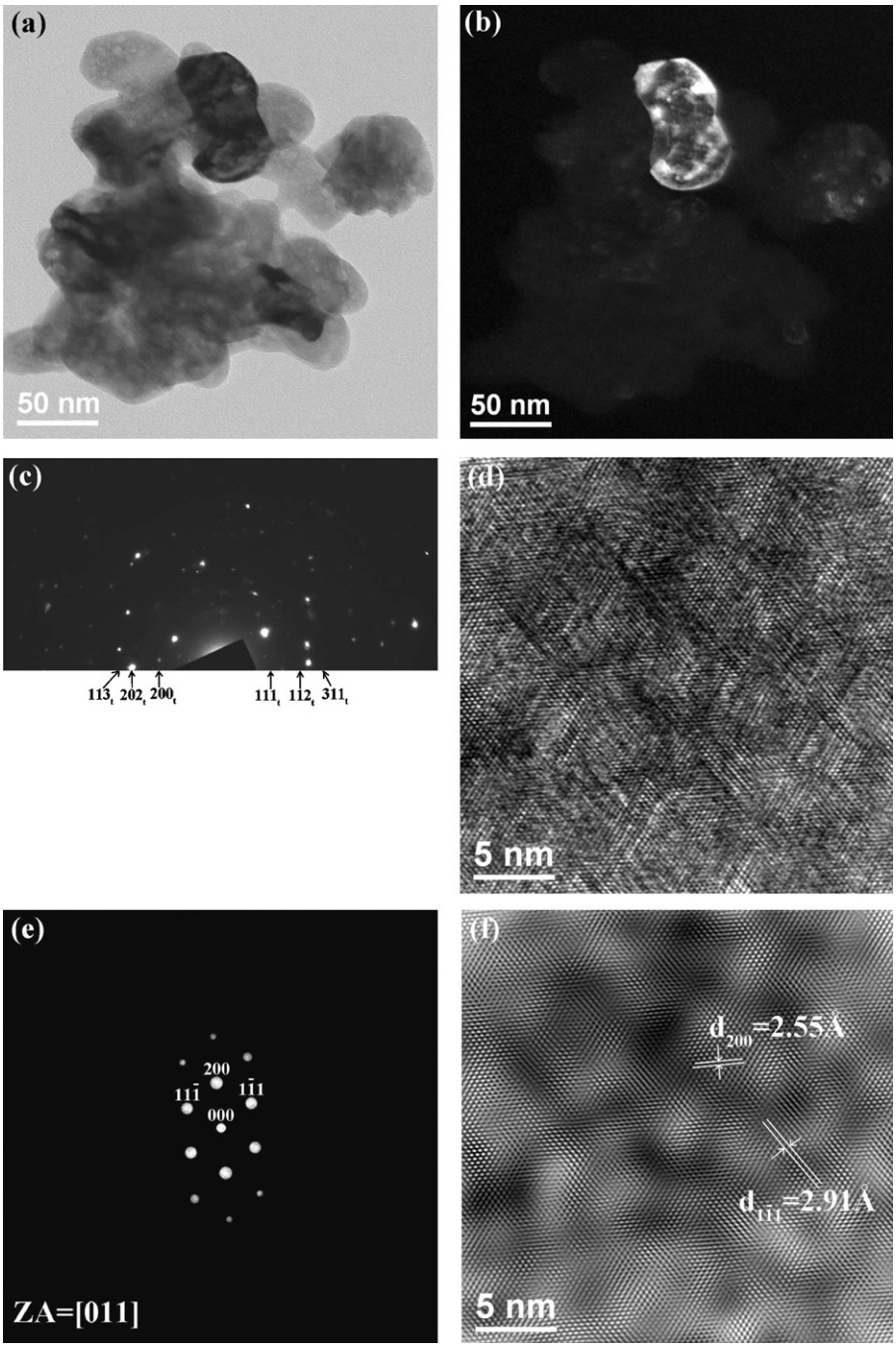

Fig. 9. Micrographs of 3Y-TZP freeze-dried precursor powders calcined at 1273 K for 5 min for the (a) BF image, (b) $(1\,1\,1)_t$ DF image, (c) SAED pattern, (d) high resolution lattice image, (e) FFT SAED pattern, and (f) IFFT atomic lattice image.

as [22,28]:

$$N = \frac{1}{\beta}\int_{T_r}^{T} I(T)dT = \frac{N_0}{\beta} \tag{5}$$

$$r = \frac{1}{\beta}\int_{T_r}^{T} U(T)dT = \frac{1}{\beta}\int_{T_r}^{T} \upsilon_0\lambda \ \exp\left(-\frac{E_c}{RT}\right)dT$$
$$= \frac{1}{\beta}\int_{T_r}^{T} \mu_0 \exp\left(-\frac{E_c}{RT}\right)dT \approx \frac{r_0}{\beta}\left(-\frac{E_c}{RT}\right) \tag{6}$$

where $I(T)$ and $U(T)$ are the rates of nucleation and crystallite growth, respectively, N_0 is the initial number of nuclei, υ_0 is the frequency of molecules climbing over energy barriers, λ is the thickness of one molecular layer of a phase, and r_0 is the initial radius of a tetragonal particle.

The two types of crystallization are nucleation of the bulk and of the surface. In nucleation, the volume fraction of crystallites, α, is presented as [29]:

$$\frac{d\alpha}{dt} = \frac{4N_0 r_0^{n-1}\mu_0}{\beta^n}(1-\alpha)\exp\left(-\frac{nE_c}{RT}\right) \tag{7}$$

As Fig. 6 shows, where $\alpha = (A_i/A)$, A is the area between the DSC curve and base line from initial crystallization temperature, T_1 to crystallization completion temperature T_2 and A_i is the partial area from T_1 to a certain temperature T. After the integral operation, Eq.

Table 1
Growth morphology parameter of n of 3Y-TZP freeze-dried precursor powders at various heating rates.

Heating rate (K min^{-1})	nE_c (kJ mol^{-1})	n
5	242.27	1.43
10	331.35	1.96
20	452.28	2.67
Average	341.97	2.02

(8) could be derived and simplified as

$$-\ln(1-\alpha) = \frac{k}{\beta^m}\exp\left(-\frac{nE_c}{RT}\right) \quad (8)$$

and further derived as [30]

$$\log[-\ln(1-\alpha)] = -\frac{nE_c}{2.303RT} - m\ \log\ \beta + const. \quad (9)$$

where n is the parameter of the growth morphology and m is the index of the crystallization mechanism. This indicates that crystallites engage in three-dimensional growth when $n=m=3$; two-dimensional growth when $n=m=2$; and one-dimensional growth when $n=m=1$ [16].

Fig. 7 shows the relationship between $\log[-\ln(1-\alpha)]$ and $(1/T)$ at various heating rates. The slopes of the fitting lines were obtained and denoted in Fig. 7. As can be seen in Eq. (9), further calculation of the slopes of the fitting lines obtained the values of growth morphology parameter, n, which are listed in Table 1. The average value of n is 2.02. Within experimental error, the average value of n was approximated as 2.0.

The relationships between $\log[-\ln(1-\alpha)]$ and $\log\beta$ at various temperatures are shown in Fig. 8. The slopes of the fitting lines for various temperatures were obtained and denoted in Fig. 8. Using Eq. (9) and these slopes, the values of crystallization mechanism index (m) were obtained and are listed in Table 2. The average value of m is 1.90. Within experimental error, the average value of m was approximated as 2.0.

According to JMA criterion, the values of n and m were approximated as 2.0, meaning that two-dimensional growth with plate-like morphology was the primary mechanism of tetragonal ZrO_2 crystallization from zirconia in 3Y-TZP freeze-dried precursor powders.

3.4. TEM microstructure of 3Y-TZP nano-powders

The TEM micrographs of the 3Y-TZP freeze-dried precursor powders calcining at 1273 K for 5 min are shown in Fig. 9. Fig. 9(a) shows the bright field (BF) image, which reveals that some two-dimensional growth crystallites were aggregated together. These two-dimensional growth crystallites corresponded with the calculated result of the crystallization mechanism as mentioned above. Fig. 9(b) shows the dark field (DF) image of the $(1\,1\,1)_t$ tetragonal crystallites. It shows that the particles were smaller than 100 nm. Fig. 9(c) shows the SAED pattern, whose index corresponds with the tetragonal ZrO_2. This result also indicates that the 3Y-TZP freeze-dried precursor powders calcining at 1273 K for 5 min could be still maintain the tetragonal phase. Fig. 9(d) shows a high resolution lattice image of a certain region. Its fast Fourier transformation (FFT) SAED pattern by fast Fourier transform (FFT) is shown in Fig. 9(e). The indexed SAED pattern shows $(1\,1\,\bar{1})$, $(1\,\bar{1}\,1)$, and planes along the [0 1 1] zone axis. According to the SAED pattern, the indexed atomic lattice image is shown in Fig. 9(f) by IFFT. It shows that the d-spacings of (2 0 0) and $(1\,\bar{1}\,1)$ were 2.55 and 2.91 Å, respectively.

Table 2
Crystallization mechanism index (m) of 3Y-TZP freeze-dried precursor powders at various temperatures.

Crystallization temp. (K)	m
775	2.03
779	1.88
783	1.79
Average	1.9

Table 3
The composition of 3Y-TZP freeze-dried precursor powders calcined at 773 and 1273 K for 5 min by TEM-EDS and the ideal composition by calculation.

Element (atomic%)	Zr	Y	O
773 K	36.83	3.20	59.97
1273 K	46.97	5.24	47.79
Ideal composition	31.70	1.96	66.34

The atomic compositions of 3Y-TZP nano-powders calcined at 773 and 1273 K for 5 min by TEM-EDS are listed in Table 3. The ideal atomic composition of 3Y-TZP nano-powders was calculated from the ideal stoichiometric $Zr_{0.97}Y_{0.06}O_{2.03}$. It can be seen in Table 3 that the O atomic ratio of the experimental 3Y-TZP was lower than the ideal O atomic ratio because the yttrium cations replaced the zirconium cations of the face centered cubic lattice sites and caused the oxygen vacancies to lead to a decrease in the O atomic ratio. In addition, the finding that yttrium atoms can be detected using TEM-EDS could be used as evidence of the generation of oxygen vacancies.

4. Conclusion

The synthesis and crystallization behavior of 3Y-TZP freeze-dried precursor powders was investigated using DSC/TG, XRD, Raman spectra, TEM, SAED and EDS. These results of this study are summarized as follows:

(1) From the estimated weight loss in the TG curve, it can be seen that the main compound of the precursor powders was $ZrO_2{\cdot}2H_2O$.
(2) The results of the XRD, Raman spectra, and SAED show the tetragonal ZrO_2 formation when the 3Y-TZP freeze-dried precursor powders calcined at 773–1273 K for 5 min. Moreover, the Raman spectrum shows that the tetragonal ZrO_2 had already formed in the 3Y-TZP freeze-dried precursor powders.
(3) The crystallization activation energy of the tetragonal phase from the 3Y-TZP freeze-dried precursor powders when using a non-isothermal method was 169.2 ± 21.9 kJ mol^{-1}.
(4) The crystallite growth morphology parameter (n) and crystallization mechanism index (m) were approximated as 2.0. This result means that the tetragonal ZrO_2 crystallites have a growth mechanism with a plate-like morphology.

Acknowledgements

The authors sincerely thank the support of the Ministry of Education, Taiwan (99-EC-17-A-08-S1-142), Professor I.M. Hung for DSC/TG, Mr. H.Y. Yao for TEM and EDS.

References

[1] E.C. Subbarao, in: A.H. Heuer, L.W. Hobbs (Eds.), Advances in Ceramics, vol. 3, The American Ceramic Society, Columbus, OH, 1981.
[2] E.C. Subbarao, Zirconia-an overview, in: A.H. Heuer, L.W. Hobbs (Eds.), Science and Technology of Zirconia, The American Ceramic Society, Columbus, OH, 1981, pp. 1–24.
[3] C. Pascual, P. Duran, Subsolidus phase equilibria and ordering in the system ZrO_2–Y_2O_3, J. Am. Ceram. Soc. 66 (1983) 23–27.
[4] R.C. Garvie, R.H.J. Hannink, R.T. Pascoe, Ceramic steel, Nature 258 (1975) 703–704.
[5] D.J. Green, R.H.J. Hannink, M.V. Swain, Transformation Toughening of Ceramics, CRC Press, Boca Raton, FL, 1989.

[6] R.H.J. Hannink, P.M. Kelly, B.C. Muddle, Transformation toughening in zirconia-containing ceramics, J. Am. Ceram. Soc. 83 (2000) 461–487.
[7] N. Claussen, J. Steeb, R.F. Pabst, Effect on induced microcracking on the fracture toughness of ceramics, Am. Ceram. Soc. Bull. 56 (6) (1977) 559–562.
[8] A.G. Evans, R.M. Cannon, Toughening of brittle solids by martensitic transformations, Acta Metall. 34 (5) (1986) 761–800.
[9] A.V. Virkar, R.L.K. Matsumoto, Ferroelastic domain switching as a toughening mechanism in tetragonal zirconia, J. Am. Ceram. Soc. 69 (1986) 224–226.
[10] G.V. Srinivasan, J.F. Jue, S.Y. Kuo, A.V. Virkar, Ferroelastic domain switching in polydomain tetragonal zirconia single crystals, J. Am. Ceram. Soc. 72 (1989) 2098–2103.
[11] C.J. Chan, F.F. Lange, M. Rühle, J.F. Jue, A.V. Virkar, Ferroelastic domain switching in tetragonal zirconia single crystals—microstructural aspects, J. Am. Ceram. Soc. 74 (1991) 807–813.
[12] E. Furlani, E. Aneggi, S. Maschio, Effects of milling on co-precipitated 3Y-PSZ powders, J. Eur. Ceram. Soc. 29 (2009) 1641–1645.
[13] I. Gonzalo-Juan, B. Ferrari, M.T. Colomer, Influence of the urea content on the YSZ hydrothermal synthesis under dilute conditions and its role as dispersant agent in the post-reaction medium, J. Eur. Ceram. Soc. 29 (2009) 3185–3195.
[14] C. Viazzi, J.P. Bonino, F. Ansart, A. Barnabé, Structural study of metastable tetragonal YSZ powders produced via a sol–gel route, J. Alloys Compd. 452 (2008) 377–383.
[15] P. Durán, J. Tartaj, J.F. Fernández, M. Villegas, C. Moure, Crystallisation and sintering behaviour of nanocrystalline Y-TZP powders obtained by seeding-assisted chemical coprecipitation, Ceram. Int. 25 (1999) 125–135.
[16] C.W. Kuo, Y.H. Lee, I.M. Hung, M.C. Wang, S.B. Wen, K.Z. Fung, C.J. Shih, Crystallization kinetics and growth mechanism of 8 mol% yttria-stabilized zirconia (8YSZ) nano-powders prepared by a sol–gel process, J. Alloys Compd. 453 (2008) 470–475.
[17] C. Piconi, G. Maccauro, Zirconia as a ceramic biomaterial, Biomaterials 20 (1999) 1–25.
[18] E.D Whitney, Observations on the nature of hydrous zirconia, J. Am. Ceram. Soc. 53 (1970) 697–698.
[19] G.K. Chuah, S. Jaenicke, B.K. Pong, The preparation of high-surface-area zirconia. II. Influence of precipitating agent and digestion on the morphology and microstructure of hydrous zirconia, J. Catal. 175 (2008) 80–92.
[20] B.K. Kim, J.W. Hahn, K.R. Han, Quantitative phase analysis in tetragonal-rich tetragonal/monoclinic two phase zirconia by Raman spectroscopy., J. Mater. Sci. Lett. 16 (1997) 669–671.
[21] K. Sato, H. Abe, S. Ohara, Selective growth of monoclinic and tetragonal zirconia nanocrystals, J. Am. Chem. Soc. 132 (2010) 2538–2539.
[22] P. Li, I.W. Chen, J.E. Penner-Hahn, Effect of dopants on zirconia stabilization-an X-ray absorption study. I. trivalent dopants, J. Am. Ceram. Soc. 77 (1994) 118–128.
[23] S. Shukla, S. Seal, R. Vij, S. Bandyopadhyay, Reduced activation energy for grain growth in nanocrystalline yttria-stabilized zirconia, Nano Lett. 3 (2003) 397–401.
[24] A Clearfield, The mechanism of hydrolytic polymerization of zirconyl solutions, J. Mater. Res. 5 (1990) 161–162.
[25] R.P. Denkewicz, K.S. TenHuisen, J.H. Adair, Hydrothermal crystallization kinetics of m-ZrO_2 and t-ZrO_2, J. Mater. Res. 5 (1990) 2698–2705.
[26] G.K. Chuah, An investigation into the preparation of high surface area zirconia, Catal. Today 49 (1999) 131–139.
[27] A Marotta, A. Buri, Kinetics of devitrification and differential thermal analysis, Thermchim. Acta 25 (1978) 155–160.
[28] G. Ertl, H. Knozinger, J. Weitkamp, Handbook of Heterogeneous Catalysis, vol. 3, WCHD-69451, Weinheim, 1997, p. 1508.
[29] K. Matusita, S. Sakka, Y. Matsui, Determination of the activation energy for crystal growth by differential thermal analysis, J. Mater. Sci. 10 (1975) 961–966.
[30] Y.F. Chen, M.C. Wang, M.H. Hon, Phase transformation and growth of mullite in kaolin ceramics, J. Eur. Ceram. Soc. 24 (2004) 2389–2397.